OXFORD

Psychoradiology, 2023, **3**, 1–12

DOI: 10.1093/psyrad/kkad017

Advance access publication date: 26 September 2023

Research Article

Aberrant single-subject morphological brain networks in first-episode, treatment-naive adolescents with major depressive disorder

Xiaofan Qiu[1], Junle Li[1], Fen Pan[2,3], Yuping Yang[1], Weihua Zhou[2,3], Jinkai Chen[2,3], Ning Wei[2,3], Shaojia Lu[2,3], Xuchu Weng[1,4,5,6], Manli Huang[2,3,7,*] and Jinhui Wang[1,4,5,6,*]

[1]Institute for Brain Research and Rehabilitation, South China Normal University, Guangzhou 510631, China
[2]Department of Psychiatry, First Affiliated Hospital, College of Medicine, Zhejiang University, Hangzhou 310013, China
[3]The Key Laboratory of Mental Disorder's Management of Zhejiang Province, Hangzhou 310013, China
[4]Key Laboratory of Brain, Cognition and Education Sciences, Ministry of Education, Guangzhou 510631, China
[5]Center for Studies of Psychological Application, South China Normal University, Guangzhou 510631, China
[6]Guangdong Key Laboratory of Mental Health and Cognitive Science, Guangzhou 510631, China
[7]Zhejiang Engineering Center for Mathematical Mental Health, Hangzhou 310003, China
*Correspondence: Jinhui Wang, jinhui.wang.1982@m.scnu.edu.cn; Manli Huang, huangmanli@zju.edu.cn

Abstract

Background: Neuroimaging-based connectome studies have indicated that major depressive disorder (MDD) is associated with disrupted topological organization of large-scale brain networks. However, the disruptions and their clinical and cognitive relevance are not well established for morphological brain networks in adolescent MDD.

Objective: To investigate the topological alterations of single-subject morphological brain networks in adolescent MDD.

Methods: Twenty-five first-episode, treatment-naive adolescents with MDD and 19 healthy controls (HCs) underwent T1-weighted magnetic resonance imaging and a battery of neuropsychological tests. Single-subject morphological brain networks were constructed separately based on cortical thickness, fractal dimension, gyrification index, and sulcus depth, and topologically characterized by graph-based approaches. Between-group differences were inferred by permutation testing. For significant alterations, partial correlations were used to examine their associations with clinical and neuropsychological variables in the patients. Finally, a support vector machine was used to classify the patients from controls.

Results: Compared with the HCs, the patients exhibited topological alterations only in cortical thickness-based networks characterized by higher nodal centralities in parietal (left primary sensory cortex) but lower nodal centralities in temporal (left parabelt complex, right perirhinal ectorhinal cortex, right area PHT and right ventral visual complex) regions. Moreover, decreased nodal centralities of some temporal regions were correlated with cognitive dysfunction and clinical characteristics of the patients. These results were largely reproducible for binary and weighted network analyses. Finally, topological properties of the cortical thickness-based networks were able to distinguish the MDD adolescents from HCs with 87.6% accuracy.

Conclusion: Adolescent MDD is associated with disrupted topological organization of morphological brain networks, and the disruptions provide potential biomarkers for diagnosing and monitoring the disease.

Keywords: adolescent major depressive disorder; structural MRI; morphological brain network; cortical thickness; support vector machine

Introduction

Major depressive disorder (MDD) is one of the most prevalent psychiatric disorders worldwide (Bromet *et al.*, 2011; Ferrari *et al.*, 2013; Otte *et al.*, 2016), which imposes significant economic and cognitive costs (Gotlib & Joormann, 2010; Greenberg *et al.*, 2015). Moreover, MDD is the leading cause of disability around the world (Vos *et al.*, 2016). In view of the global prevalence and burden of MDD, it is worthwhile working out the neural mechanism of the disease to help its diagnosis, prevention, and prognosis.

Benefiting from advances in noninvasive neuroimaging techniques and sophisticated analytical methods, great progress has been made in the last decade in mapping brain structural and functional alterations in MDD. In particular, connectomics analysis of multimodal magnetic resonance imaging (MRI) data reveals that MDD is related to disrupted topological organization of large-scale brain networks (Chen *et al.*, 2017; Jiang *et al.*, 2019; Korgaonkar *et al.*, 2020; Li *et al.*, 2022; Shin *et al.*, 2018; Yao *et al.*, 2019; Zhang *et al.*, 2021), prompting a conceptual proposal to view MDD as a network dysfunctional syndrome (Gong & He, 2015). However, these studies mainly focus on adult patients. Compared with adult MDD, adolescent MDD is associated with an increased risk for the recurrence of MDD during adulthood (Nardi *et al.*, 2013) and a higher rate of suicide (Johnson *et al.*, 2018). Moreover, since adolescence is a period of marked physical, mental and brain development (Balvin & Banati, 2017; Belcher *et al.*, 2021; Lenroot & Giedd, 2006), MDD in this period could lead to serious social and educational impairments and misbehaviors (Thapar *et al.*, 2012). Therefore, researchers have begun to

Received: 5 June 2023; **Revised:** 13 September 2023; **Accepted:** 20 September 2023

turn their attention to brain network dysfunction in adolescent MDD.

Currently, several studies have been conducted to examine functional brain networks derived from functional MRI or structural brain networks constructed with diffusion MRI in adolescents with MDD (Chu *et al.*, 2018; Ho *et al.*, 2017; Sacchet *et al.*, 2016; Tymofiyeva *et al.*, 2019; Wu *et al.*, 2020). In addition to these two types of brain network, single-subject morphological brain networks based on structural MRI provide another important way to study human brain networks (for a recent review, see Cai *et al.*, 2023). A major advantage of single-subject morphological brain networks is their high test-retest reliability (Jiang *et al.*, 2017; Kong *et al.*, 2015; Li *et al.*, 2017, 2021c; Tijms *et al.*, 2012; Wang *et al.*, 2016, 2018; Yin *et al.*, 2023; Yu *et al.*, 2018; Zhao *et al.*, 2021), which confers the potential to establish reliable biomarkers in brain diseases. More importantly, single-subject morphological brain networks are increasingly demonstrated to have biological underpinnings by revealing their associations with various properties of cortical microarchitecture, such as gene expression, cytoarchitectonic classification, and myelin content (Li *et al.*, 2022; Sebenius *et al.*, 2023; Seidlitz *et al.*, 2018; Yang *et al.*, 2021; Zhao *et al.*, 2021). Thus, single-subject morphological brain networks are a reliable, biologically plausible approach to study cortical organization from an integrated perspective. To date, single-subject morphological brain networks have been used to study various brain diseases, including adult MDD (Chen *et al.*, 2017; Gao *et al.*, 2023; Li *et al.*, 2021, 2023), stroke (Lv *et al.*, 2021), and multiple sclerosis (Casas-Roma *et al.*, 2022; Collorone *et al.*, 2020; Yang *et al.*, 2023). With respect to adolescent MDD, however, it is largely unknown regarding whether single-subject morphological brain networks are disrupted and whether the alterations (if observed) are related to clinical manifestations and cognitive deficits of patients.

In this study, we aimed to disclose topological alterations of single-subject morphological brain networks in adolescent MDD, and further examine clinical and cognitive relevance of the alterations. To this end, we collected structural MRI and neuropsychological data from 25 first-episode, treatment-naive adolescent MDD patients and 19 age-, sex-, and education-matched healthy controls (HCs). Single-subject morphological brain networks were constructed using our previous surface-based single-subject method (Li *et al.*, 2021c; Lv *et al.*, 2021). Topological organizations of the networks were characterized by graph-based network measures, whose between-group differences were examined with permutation testing. Between-group differences in regional morphology and interregional morphological similarity were also compared. For observed alterations, their associations with clinical and neuropsychological variables were further examined in the patients. Finally, we tested whether the alterations can be used to classify the adolescent MDD patients from HCs using support vector machine (SVM). We hypothesized that single-subject morphological brain networks were disrupted in adolescent MDD patients, and the disruptions could account for clinical features and cognitive disturbances of the patients and distinguish the patients from HCs.

Materials and Methods

Participants

A total of 46 participants were recruited in the current study, including 25 first-episode, treatment-naive adolescents with MDD and 21 age-, sex-, and education-matched HCs. The MDD patients were recruited from the Department of Mental Health at the First Affiliated Hospital, College of Medicine, Zhejiang University. Matched healthy volunteers were recruited from the local community via advertisements. MDD was diagnosed according to the Diagnostic and Statistical Manual of Mental Disorders, IV Edition (DSM-IV) criteria for first-episode current unipolar MDD, which was assessed by two professional psychiatrists using structured clinical interviews based on the DSM-IV. The inclusion criteria included: (i) aged 13 to 18; (ii) right handedness; (iii) Han ethnicity; (iv) IQ > 80; and (v) scored at least 40 on the Children's Depression Rating Scale-Revised (CDRS-R) (Poznanski *et al.*, 1984) for the patients. The exclusion criteria were as follows: (i) MDD patients with any form of treatment prior to the study; (ii) significant medical illness; (iii) a history of neurological and psychiatric disorders; (iv) abnormal signals in conventional MRI imaging; (v) any other current psychiatric axis-I or axis-II disorders (except MDD in the patients); (vi) current alcohol and drug abuse; (vii) pregnant women; and (viii) contraindications for MRI scanning, including metallic implants, retractors or braces, and claustrophobia. Two HCs were excluded due to poor image quality. Finally, 44 adolescents (25 MDD and 19 HCs) were included.

The study was approved by the ethics committee of the First Affiliated Hospital of the College of Medicine of Zhejiang University and conducted in accordance with the Code of Ethics of the World Medical Association (Declaration of Helsinki). To make sure that the adolescent participants felt respected and thus better engaged in this study, they were informed of some details beforehand and gave their consent as well as their parents or legal guardians before the study began.

Clinical and neuropsychological measurements

In the current study, all participants underwent a battery of clinical and neuropsychological tests. Specifically, clinical tests, assessing the severity of depressive symptoms, included the 17-item Hamilton Depression Rating Scale (HAMD) (Hamilton, 1967) and the Children's Depression Rating Scale, revised version (CDRS-R) (Poznanski *et al.*, 1984). Neuropsychological tests included the Wisconsin Card Sorting Test (WCST) (Monchi *et al.*, 2001), Continuous Performance Test (CPT) (Rosvold *et al.*, 1956), Trail-making test (TMT) (Arnett & Labovitz, 1995), and Stroop Color Word Test (Stroop, 1935). These tests were chosen since they had been frequently used in previous studies of adult and/or adolescent MDD, and were of good practicability (Doom *et al.*, 2021; Huang *et al.*, 2012; Pan *et al.*, 2020).

Image acquisition

All MRI data were acquired using a Philips Achieva 3.0 T TX MRI system (Philips Healthcare, Netherlands) with an eight-channel head coil array. The 3D high-resolution T1-weighted images were acquired axially using a fast field echo sequence with the following imaging parameters: 150 slices, repetition time (TR) = 7.5 ms, echo time (TE) = 3.7 ms, flip angle (FA) = 8°, slice thickness/gap = 1/0 mm, voxel size = 1 × 1 × 1 mm^3, matrix = 240 × 240 and field of view (FOV) = 240 × 240 mm^2.

Data preprocessing

Data preprocessing of structural images was performed using the Computational Anatomy Toolbox (CAT12, http://www.neuro.uni-jena.de/cat) based on Statistical Parametric Mapping software (SPM12, http://www.fil.ion.ucl.ac.uk/spm/software/spm12/). CAT12 offers a fast and reliable approach for analysis of cerebral surface-based morphometry, such as cortical thickness (CT), fractal dimension (FD), gyrification index (GI), and sulcus depth

(SD). Briefly, individual structural images were first segmented into gray matter, white matter, and cerebrospinal fluid. During the segmentation process, we used the standard tissue probability maps as provided in the SPM12 to initialize the segmentation, the ICBM space template (East Asian brains) for affine regularization, and an optimized shooting approach for spatial registration (Ashburner & Friston, 2011). According to the CAT12 manual, we did not use customized tissue probability maps, which are only recommended for data obtained in young children. Then, estimation of CT and reconstruction of the central surface were conducted based on the projection-based thickness method, which allows the handling of partial volume information, sulcal blurring, and sulcal asymmetries (Dahnke *et al.*, 2013). FD, GI, and SD were further calculated with default parameter settings based on the constructed central surface. Finally, individual morphological maps of CT, FD, GI, and SD were resampled into the common fsaverage template and smoothed using a Gaussian kernel with 12-mm full-width at half-maximum for the CT maps and 25-mm full -width at half-maximum for the other maps. According to the recommendations of the CAT12 manual, the usage of larger smoothing kernel sizes for the FD, GI, and SD maps was due to the underlying nature of these folding measures that reflected contributions from both sulci and gyri. Therefore, the smoothing kernel size should exceed the distance between a gyral crown and a sulcal fundus.

Construction of morphological brain networks

In this study, morphological brain networks were constructed using our previous method (Li *et al.*, 2021c; Lv *et al.*, 2021). First, the Human Connectome Project multi-modal parcellation atlas (Glasser *et al.*, 2016) was used to parcel the cerebral cortical surface into 360 regions of interest (ROI), each of which represented a node. Then, for each morphological index, all values within each ROI were extracted and used to estimate regional probability density function by the kernel density estimation (MATLAB function: ksdensity). Subsequently, the probability density functions were converted to corresponding probability distribution functions (PDFs). For two regions with PDFs P and Q, respectively, the Jensen–Shannon divergence (JSD), a variation of the Kullback–Leibler divergence (KLD), was calculated as:

$$JSD\left(P \parallel Q\right) = \frac{1}{2}KLD\left(P \parallel M\right) + \frac{1}{2}KLD\left(Q \parallel M\right)$$

$$KLD\left(P \parallel Q\right) = \sum_{i=1}^{n} P\left(i\right) log\frac{P\left(i\right)}{Q\left(i\right)}$$

where $M = \frac{1}{2}(P + Q)$, and n is the number of sample points (2^8 in the current study) (H. Wang *et al.*, 2016). Finally, the morphological connectivity (MC) between two regions was defined as:

$$MC_{(P,Q)} = 1 - \sqrt{JSD\left(P \parallel Q\right)}$$

These procedures resulted in four sets of 360 × 360 MC matrices [i.e. CT-based networks (CTNs), FD-based networks, GI-based networks, and SD-based networks].

Network analysis of morphological brain networks

Threshold selection

For the MC matrices derived here, a sparsity-based thresholding procedure was employed to convert each of them to a set of binary networks, wherein sparsity is defined as the number of actual edges divided by the total number of possible edges in a network. By applying a subject-specific MC threshold to individual MC matrices, the sparsity-based thresholding procedure ensures the same number of edges or network cost for the resultant networks across participants. As there are no definitive ways to determine a single sparsity value, the MC matrices were repeatedly thresholded over a consecutive sparsity range from 0.02 to 0.4 (interval of 0.02). The sparsity range was selected to ensure that the resultant networks have sparse properties (Achard, 2006; He *et al.*, 2007; Wang *et al.*, 2009) and are estimable for small-world attributes (Watts & Strogatz, 1998). In addition to the binary networks, we also derived their corresponding weighted networks to examine the reproducibility of our findings by taking the MC of supra-threshold edges into account.

Network measure calculation

In this study, 4 (morphological index: CT/FD/GI/SD) × 2 (network type: binary/weighted) × 20 (sparsity level: 0.02–0.4) morphological networks were constructed for each participant. For each network, we calculated graph-based global (clustering coefficient, C_p, characteristic path length, L_p, normalized C_p, and normalized L_p) and nodal (degree, efficiency, betweenness, eigenvector, and PageRank) properties with the GRETNA toolbox (Wang *et al.*, 2015). Detailed formulas and interpretations of these measures can be found elsewhere (Rubinov & Sporns, 2010). Given that all graph-based network measures were calculated as functions or curves of sparsity, we further computed the area under the curve for each measure to provide sparsity-independent summary scalars for subsequent statistical analysis.

Statistical analysis

Between-group differences in demographic, clinical and neuropsychological variables

For discrete sex data, a χ^2 test was used to examine between-group differences. For other continuous variables, Lilliefors tests were first used to determine whether they followed normal distribution within each group. For variables conforming to normal distribution within both the patient and control groups, two-sample *t*-tests were used to test their between-group difference; otherwise, Wilcoxon rank sum tests were used instead.

Between-group differences in MRI-based variables

For each morphological index, between-group differences were examined for the mean morphological value within each ROI, MC between each pair of ROIs and each graph-based network measure with non-parametric permutation test (10 000 times) based on the *t* statistics derived from two-sample *t*-tests. During the comparisons, age, sex, and education were treated as covariates. A false discovery rate (FDR) procedure was used to correct for multiple comparisons for intraregional mean morphological value (across 360 ROI), for each nodal property (across 360 ROI), and for global network properties (across four properties). For interregional MC, a threshold-free network-based statistics (TFNBS) method (Baggio *et al.*, 2018) was used to correct for multiple comparisons across all connections. These corrections were performed within each type of single-subject morphological brain networks. For the FDR procedure, the first step involved the sorting of the original *P* values (e.g. 360 *P* values derived from between-group comparisons of nodal degree for binary CTNs) in ascending order. Then, the *k*th element in the ascending *P* values (p_k) was determined according to the following formula, which was the threshold that would restrict the expected proportion of type

I errors to $q < 0.05$:

$$k = \max\left\{i : \ p_i \le \frac{i}{n} \times 0.05 / \left(\sum_{j=1}^{n} 1/j\right)\right\}$$

where n denotes the number of tests. All tests with a P value equal or smaller than p_k were considered significant.

Relationships between MRI-based measures and clinical and neuropsychological variables

For MRI-based measures showing significant alterations in the adolescent MDD patients, Spearman partial correlation was used to examine their relationships with clinical variables (age of onset, course of illness, HAMD, and CDRS-R) in the patients. Effects of sex, age, and education were controlled for the MRI-based measures. Similarly, Spearman partial correlation analyses were performed between the MRI-based measures and neuropsychological tests showing significant alterations in the adolescent MDD patients with sex, age, and education as covariates. The FDR procedure was used to correct for multiple comparisons across all correlation analyses between 17 MRI-based measures showing significant alterations in the patients and eight clinical and neuropsychological variables ($17 \times 8 = 136$ correlation analyses).

Classification

A linear kernel SVM algorithm was implemented to distinguish the adolescent MDD from HCs with all network properties derived from both the binary and weighted CTNs as initial features. A 10-fold cross-validation procedure was used to evaluate the out-of-sample prediction performance. The ratio of the sample size in the training set to the test set was ~9:1. More specifically, the sample sizes were 40 versus 4 in 6 out of the 10 folds and 39 versus 5 in the other folds. In each fold, a SVM classifier was trained based on features that exhibited significant between-group differences ($P < 0.05$; permutation test) in the training set. The classifier was then applied to the unseen test set to predict the group labels of left-out participants. The predictive ability of the SVM classifier was assessed by means of accuracy, sensitivity, and specificity:

$$Accuracy = \frac{TP + TN}{TP + TN + FP + FN}$$
$$Sensitivity = \frac{TP}{TP + FN}$$
$$Specificity = \frac{TN}{TN + FP}$$

where TP, TN, FP, and FN represent true positive, true negative, false positive, and false negative, respectively. To robustly assess these measures, the 10-fold cross-validation procedure was repeated 100 times and the resultant mean accuracy, sensitivity, and specificity were calculated. Meanwhile, features that were consistently selected across all folds and repeats were recorded together with their weights in contributing to the SVM classifiers averaged across the folds and repeats. Finally, to evaluate whether the trained SVM classifiers performed by chance, a P value was separately estimated for the accuracy, sensitivity, and specificity by generating corresponding empirical null distributions based on the initial features with reshuffled group labels (1000 times). Notably, before the classification procedures, effects of age, sex, and education were regressed out from all the features via multiple linear regression.

Table 1: Demographic and clinical characteristics.

	MDD	HCs	P value
Gender (M/F)	8/17	6/13	0.976[a]
Age (years)	16 (2.25)	16 (1)	0.250[b]
Education (years)	9 (2.25)	9.32 ± 1.67	0.961[b]
HAMD	25.56 ± 5.11	0 (2)	<0.001[b]
CDRS-R	71.63 ± 12.59	17 (2.75)	<0.001[b]
Age of onset (years)	16 (3.25)	–	–
Course of illness (months)	6 (10)	–	–

Data are presented as mean ± standard deviation or median (interquartile range) depending on whether the variables are normally distributed (Lilliefors test). M, male; F, female; HAMD, Hamilton Depression Scale; CDRS-R, Children's Depression Rating Scale-Revised.
[a]The P value was obtained by a chi-square test.
[b]The P values were obtained by Wilcoxon rank sum tests.

Results

Demographic, clinical, and neuropsychological variables

The demographic and clinical characteristics of all participants are shown in Table 1. There were no significant differences in age, sex, or education between the two groups (all $P > 0.05$). However, compared with the HCs, the adolescent MDD patients had significantly higher HAMD and CDRS-R scores (both $P < 0.001$). For neuropsychological variables, the adolescent MDD patients showed worse performance on the TMT B, SCWT A, SCWT B, and SCWT C than the HCs (all $P < 0.05$) (Table 2).

Alternations in intraregional morphological value in adolescent MDD

No significant differences were found between the patients and HCs in the mean morphological value within any region regardless of the morphological index ($P > 0.05$, FDR corrected).

Alternations in interregional MC in adolescent MDD

No significant differences were found between the patients and HCs in the MC between any pair of regions regardless of the morphological index ($P > 0.05$, TFNBS corrected).

Alternations in topological organization of single-subject morphological brain networks in adolescent MDD

Topological alterations in the adolescent MDD patients were observed only in the CTNs ($q < 0.05$). Specifically, compared with the HCs, the adolescent MDD patients exhibited significantly higher nodal degree ($t_{39} = 4.097$, $P = 2.3 \times 10^{-4}$, $q = 0.037$) and eigenvector ($t_{39} = 3.743$, $P = 3.3 \times 10^{-4}$, $q = 0.034$) in the left primary sensory cortex, lower nodal eigenvector ($t_{39} = -4.345$, $P = 1.3 \times 10^{-4}$, $q = 0.034$) in the left parabelt complex, lower nodal degree ($t_{39} = -4.134$, $P = 1.5 \times 10^{-4}$, $q = 0.037$) and efficiency ($t_{39} = -4.211$, $P = 1.0 \times 10^{-4}$, $q = 0.018$) in the right area PHT, and lower nodal eigenvector ($t_{39} = -3.854$, $P = 2.2 \times 10^{-4}$, $q = 0.034$) in the right ventral visual complex for the binary CTNs (Fig. 1). Analysis of the weighted CTNs generated largely similar results (Fig. 2). That is, the adolescent MDD patients showed significantly higher nodal efficiency ($t_{39} = 4.061$, $P = 2.3 \times 10^{-4}$, $q = 0.026$) and eigenvector ($t_{39} = 3.724$, $P = 3.2 \times 10^{-4}$, $q = 0.033$) in the left primary sensory cortex, lower nodal eigenvector ($t_{39} = -4.360$, $P = 0.8 \times 10^{-4}$, $q = 0.025$) and efficiency ($t_{39} = -3.587$, $P = 5.2 \times 10^{-4}$, $q = 0.029$) in the left parabelt complex, lower nodal

Table 2: Neuropsychological characteristics.

	MDD	HCs	P value
Wisconsin Card Sorting Test			
Total number of trials	48 (2.5)	48 (3)	0.702[a]
Number of correct trials	35 (9.75)	36 (8)	0.673[a]
Total number of errors	15.30 ± 10.50	14.39 ± 8.51	0.765[b]
Number of perseverative errors	10.00 ± 7.33	8.94 ± 7.70	0.657[b]
Number of random errors	4 (3)	5.72 ± 3.27	0.339[a]
Number of completed categories	5 (3)	5 (2)	0.373[a]
Continuous Performance Test			
1	11 (1.75)	11 (0)	0.423[a]
2	9 (3)	9.28 ± 2.82	0.894[a]
3	11 (3)	12 (1)	0.113[a]
Trail Making Test			
A	42.30 ± 13.09	32 (10.53)	0.057[a]
B	82 (27.25)	68.93 ± 15.36	0.001[a]
Stroop Color-Word Test			
A	46.30 ± 10.22	40.19 ± 8.59	0.049[b]
B	72 (17.5)	62.41 ± 13.29	0.008[a]
C	120 (41.25)	93.29 ± 27.87	0.008[a]
Interference	45 (27.75)	30.88 ± 23.08	0.095[a]

Data are presented as mean ± standard deviation or median (interquartile range) depending on whether the variables are normally distributed (Lilliefors test). Of note, data of the neuropsychological tests were missing for two patients and one control.
[a]The *P* values were obtained by Wilcoxon rank sum tests.
[b]The *P* values were obtained by two-sample *t*-tests.

eigenvector ($t_{39} = -3.768$, $P = 5.5 \times 10^{-4}$, $q = 0.041$), efficiency ($t_{39} = -4.210$, $P = 0.6 \times 10^{-4}$, $q = 0.013$) and betweenness ($t_{39} = -4.316$, $P = 0.3 \times 10^{-4}$, $q = 0.011$) in the right area PHT, and lower nodal eigenvector ($t_{39} = -3.845$, $P = 2.9 \times 10^{-4}$, $q = 0.033$) and efficiency ($t_{39} = -3.662$, $P = 6.8 \times 10^{-4}$, $q = 0.030$) in the right ventral visual complex. In addition, lower nodal eigenvector ($t_{39} = -3.678$, $P = 6.5 \times 10^{-4}$, $q = 0.041$) and efficiency ($t_{39} = -3.827$, $P = 4.9 \times 10^{-4}$, $q = 0.029$) were observed in the patients in the right perirhinal ectorhinal cortex. No significant between-group differences were found in any global properties for either the binary or weighted CTNs ($q > 0.05$).

Relationships between altered nodal centralities and clinical/neuropsychological variables in adolescent MDD

No significant correlations were observed for altered nodal centralities in the CTNs with any clinical or neuropsychological variables in the adolescent MDD patients ($q > 0.05$). Using a uncorrected significance level of $P < 0.05$, nodal eigenvector (binary CTNs: $rho = -0.565$, $P = 0.010$, $q = 0.623$; weighted CTNs: $rho = -0.550$, $P = 0.012$, $q = 0.593$) and efficiency (weighted CTNs: $rho = -0.535$, $P = 0.015$, $q = 0.593$) of the left parabelt complex were negatively correlated with the SCWT A, nodal eigenvector (binary CTNs: $rho = 0.425$, $P = 0.043$, $q = 0.593$; weighted CTNs: $rho = 0.436$, $P = 0.038$, $q = 0.602$) of the left parabelt complex was positively correlated with the onset age of illness, nodal eigenvector (weighted CTNs: $rho = 0.548$, $P = 0.008$, $q = 0.602$) and efficiency (weighted CTNs: $rho = 0.549$, $P = 0.008$, $q = 0.602$) of the right perirhinal ectorhinal cortex were positively correlated with the course of illness, and nodal betweenness (weighted CTNs: $rho = 0.532$, $P = 0.016$, $q = 0.602$) of the right area PHT was positively correlated with the SCWT C (Fig. 3).

Classification results

The SVM classifiers based on all network properties from both the binary and weighted CTNs exhibited good performance in distinguishing the adolescent MDD patients from HCs (accuracy = 0.876, $P < 0.001$; sensitivity = 0.963, $P < 0.001$; specificity = 0.762, $P < 0.001$; AUC = 0.958, $P < 0.001$). Out of all network properties, 73 were consistently selected to train the SVM classifiers across all folds and repeats (Fig. 4). The properties were mainly involved in frontal and parietal regions in addition to those showing significant between-group differences as mentioned before.

Discussion

In this study, we explored the topological alterations of morphological brain networks in adolescents with MDD. Compared with the HCs, the adolescents with MDD showed increased nodal centralities in parietal but decreased nodal centralities in temporal regions in the CTNs. The alterations were related to cognitive impairments and clinical characteristics of the patients, and could distinguish the patients from HCs. These findings provide preliminary evidence for network dysfunction in adolescent MDD from the perspective of morphological brain networks, and may help clinical diagnosis of the disease and monitor cognitive deficits as the disease progresses. Nevertheless, we highlight that the findings observed in this study should be explained with cautions owing to the small sample size and uncorrected nature of the correlating results.

We found that the adolescent MDD patients exhibited increased nodal centralities in the left primary sensory cortex. The primary sensory cortex is located in the postcentral gyrus, the primary somatosensory cortex that responds to somatosensory stimuli specifically (Glasser *et al.*, 2016). MDD is known to cause alterations in various sensorimotor functions, such as reduced visual contrast sensitivity (Bubl *et al.*, 2010), altered pain tolerance (Thompson *et al.*, 2016), and reduced heartbeat perception accuracy (Pollatos *et al.*, 2009). In a recent study, Ray and colleagues showed that altered effective connectivity in sensorimotor regions might act as a promising and quantifiable candidate marker

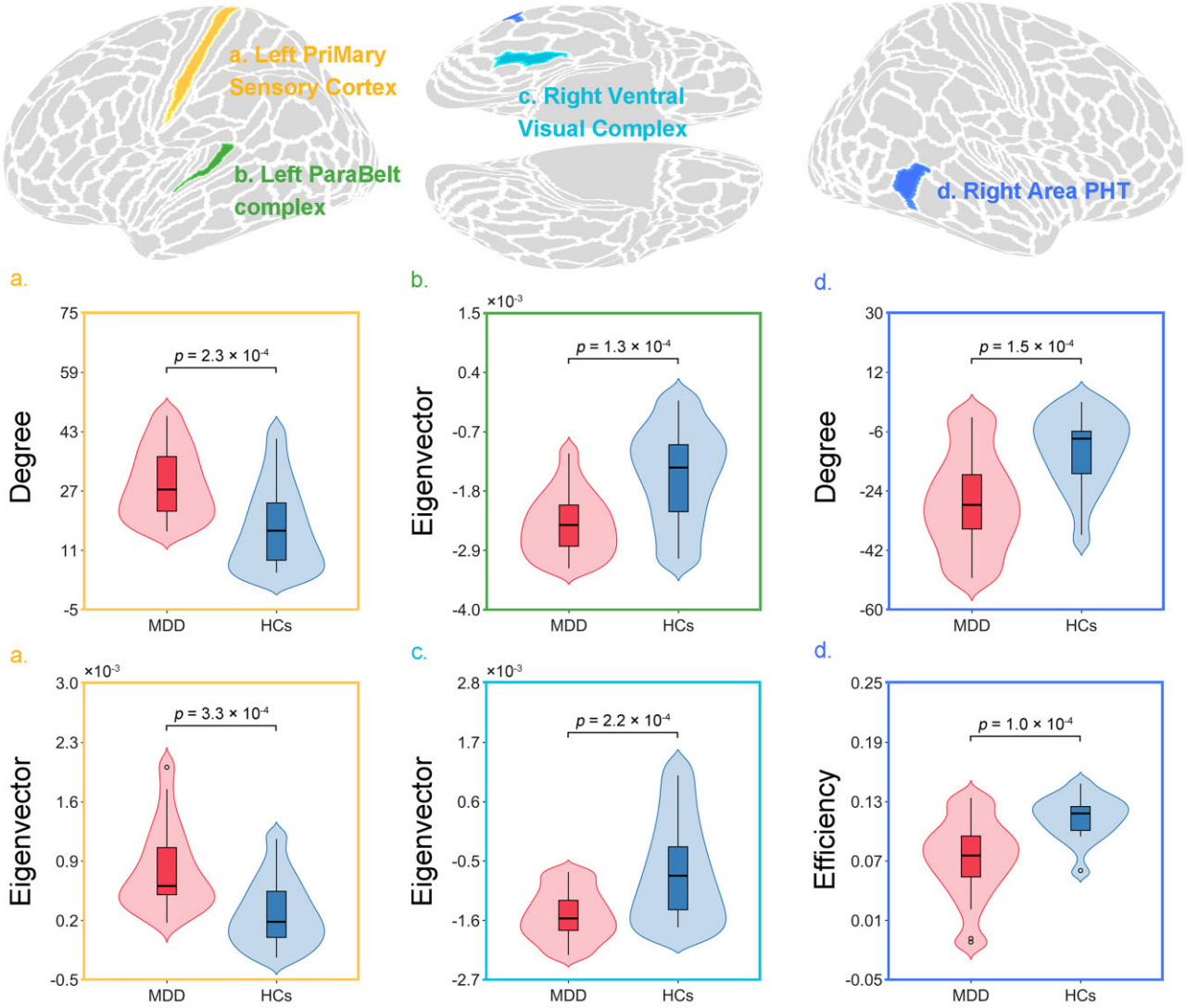

Figure 1: Between-group differences in nodal properties derived from the binary CTNs. Four regions were identified to show altered nodal centralities in the adolescent MDD patients. Values in the violin plots are residuals of the nodal centralities after removing the effects of age, sex, and education via multiple linear regression.

of depression severity and treatment response (Ray *et al.*, 2021). Here, our finding implies that network dysfunction of sensorimotor components may occur in adolescent MDD as well. More specifically, our finding suggests a more interactive state of the left primary sensory cortex in adolescent MDD as the higher nodal centralities mean more central roles in maintaining the integrity of and coordinating information flow within a network. Presumably, this might be the consequence of compensatory adaption to ensure global function of patients' brains, and is consistent with a previous study showing increased functional homogeneity in the postcentral gyrus in adolescent MDD (Mao *et al.*, 2020). However, morphological comparisons revealed cortical thinning in the postcentral gyrus in adolescent MDD (Fallucca *et al.*, 2011), and the thinning was linked to enhanced vulnerability to future depression during the adolescent-young adulthood transition (Meruelo *et al.*, 2021). The discrepancy may suggest different mechanisms between structural and functional and between local and connective alterations of sensorimotor regions in adolescent MDD.

In addition to the increased nodal centralities, the adolescent MDD patients were found to show decreased centralities in four temporal regions (the left parabelt complex, right area PHT, right ventral visual complex and right perirhinal ectorhinal cortex). The parabelt complex, located in the superior temporal gyrus, contributes to the early auditory cortex as the higher-order field surrounding the primary auditory core region and belt areas (Kaas & Hackett, 2000; Saenz & Langers, 2014), and is activated in overt reading paradigm (Zachlod *et al.*, 2020). A previous study showed that patients with MDD exhibited a lower overt reading speed (Ahern & Semkovska, 2017). Thus, the decreased nodal centralities in the parabelt complex may be related to the impairments of overt reading in adolescent MDD. This speculation sounds plausible given the negative correlation between nodal centralities in the parabelt complex and the reaction time in the Stroop Color Word Test (word reading condition) in the adolescents with MDD, although the correlation did not pass multiple comparison correction. Notably, a previous gray matter covariance network study in adult MDD found lower nodal centrality in the superior temporal gyrus, in which the parabelt complex is located (Singh *et al.*, 2013). The consistency may imply a common neural mechanism shared by adult and adolescent MDD that under-

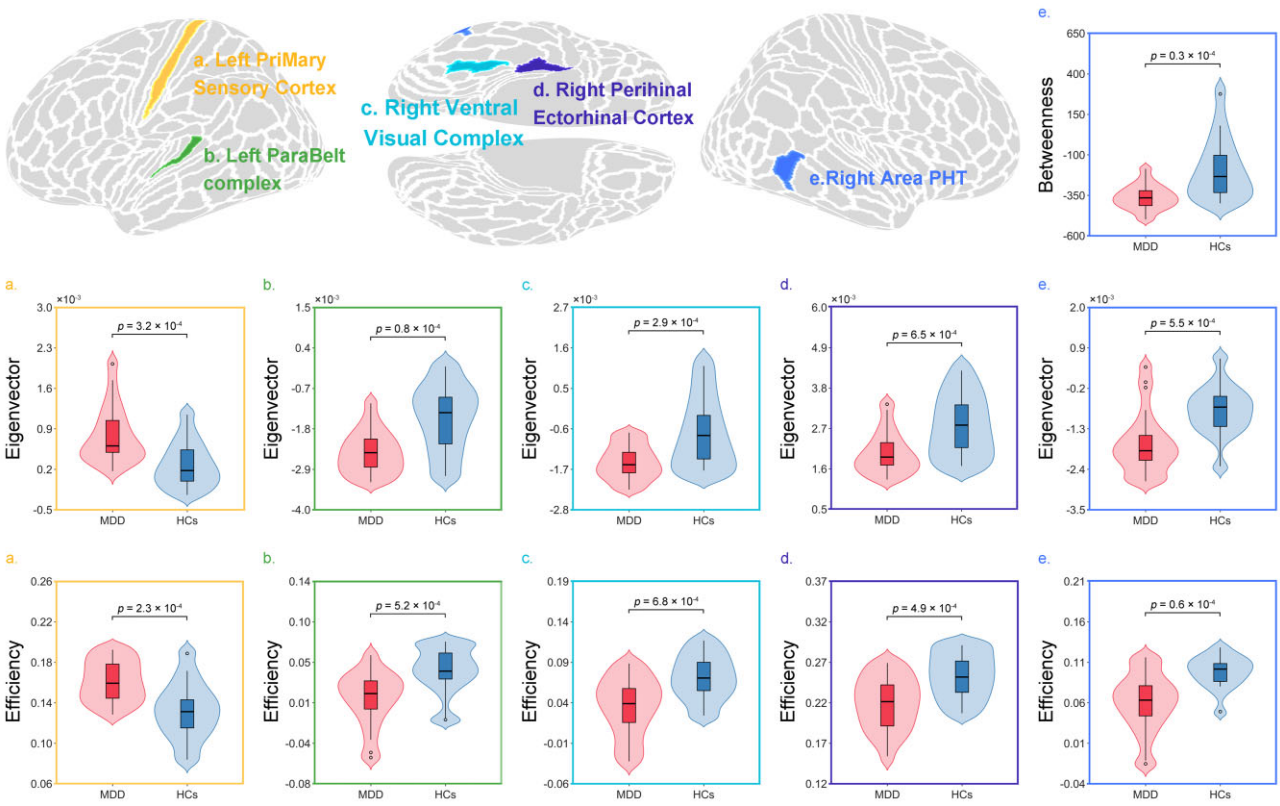

Figure 2: Between-group differences in nodal properties derived from the weighted CTNs. Five regions were identified to show altered nodal centralities in the adolescent MDD patients. Values in the violin plots are residuals of the nodal centralities after removing the effects of age, sex, and education via multiple linear regression.

lies dysfunctional visual stimuli processing and overt reading in patients.

Area PHT is located in the posterior middle temporal gyrus, and is strongly associated with the task positive network, wherein regions show consistent activations across different tasks particularly those involving attention (Blumenfeld, 2016; Glasser *et al.*, 2016). The decreased nodal centralities in the area PHT thus may reflect distraction and difficulty of adolescents with MDD in focusing on targets. This finding is consistent with a previous functional brain network study showing decreased nodal centralities in the middle temporal gyrus in first-episode adolescents with MDD (Wu *et al.*, 2020). Thus, it seems that the middle temporal gyrus, in particular the area PHT, may play an important role in understanding why adolescents with MDD typically fail to orient their attention to important environmental cues.

Finally, the ventral visual complex and the perirhinal ectorhinal cortex are both located in the fusiform gyrus, with the former activated in place- and tool-related working memory tasks (Glasser *et al.*, 2016; Weiner *et al.*, 2014), whereas the latter is activated in the face-related working memory tasks (Glasser *et al.*, 2016). Despite diverse responses to different types of visual stimuli, both the sub-regions of the fusiform gyrus contribute to visual working memory (Glasser *et al.*, 2016), which requires processing of visual information (Baddeley, 1992). Thus, we speculate that the decreased nodal centralities in the entral visual complex and the perirhinal ectorhinal cortex may suggest impaired visual working memory in adolescent MDD. These findings are consistent with a previous functional MRI study showing hypo-activation in the fusiform gyrus in facial emotion identification task in adolescent MDD (Ho *et al.*, 2016). However, in adult MDD a voxel-based meta-analysis of functional MRI studies revealed stronger response in the fusiform gyrus in working memory tasks, and the increased response became more evident in patients with more severe depression symptoms (X. Wang *et al.*, 2021). The discrepancy implies differential roles of the fusiform gyrus in contributing to impaired visual working memory, in particular face-related visual processing, between adolescent and adult MDD. Future direct comparison studies may help clarify this issue. It should be noted that we found a positive correlation between nodal centralities of the perirhinal ectorhinal cortex and course of illness of the patients. That is, as the course of illness increases, nodal centralities increase and the deviation to HCs decreases in the perirhinal ectorhinal cortex. This counterintuitive positive correlation need further confirmation in future studies.

It should be emphasized that all these temporal regions are engaged in emotional processing. Although the most investigated brain regions related to emotional processing are prefrontal and limbic areas (Maletic *et al.*, 2007), temporal regions are increasingly recognized to involve in the higher stages of emotional processing, such as appraisal and reactivity (Leppänen, 2006). A recent study proposed that adolescent MDD was more subject to disruptions in primary emotional processes (e.g. perception) (Li & Wang, 2021), which is mainly related to the primary and secondary visual cortices, fusiform gyrus, and superior temporal gyrus (Leppänen, 2006; Li & Wang, 2021). In adolescent MDD, hyperactivities in the superior and middle temporal gyri have been reported during emotional processing (Li & Wang, 2021). Therefore, presumably the decreased nodal centralities in the temporal regions as observed in this study may be relevant to the biased emotional

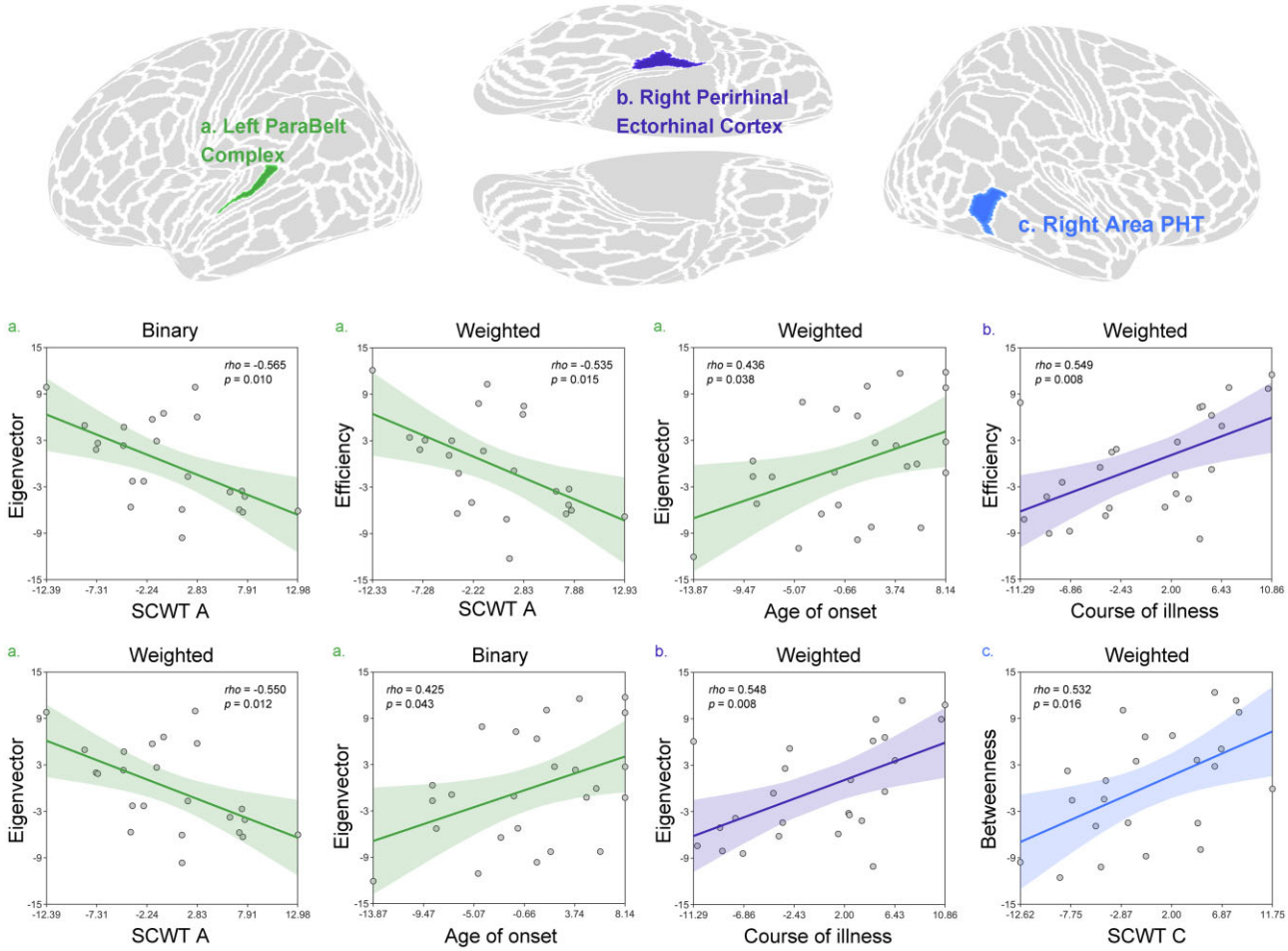

Figure 3: Relationships between nodal properties derived from the CTNs and clinical and neuropsychological variables in the adolescent MDD patients. Values in the scatter plots were residuals of the nodal centralities and clinical and neuropsychological variables after removing the effects of age, sex, and education via multiple linear regression. SCWT, Stroop Color-Word Test.

processing in adolescent MDD. Future studies may provide further insights into this speculation by examining the relationships of these regions with emotional processing capacity in adolescents with MDD.

In this study, topological alterations in adolescent MDD were observed only in the CTNs but not FD-based networks, GI-based networks, or SD-based networks. This may be partially due to different cellular mechanisms between CT and folding-based morphological indices (i.e. FD, GI, and SD). Specifically, CT reflects the size, density, and arrangement of cells in the cerebral cortex (Narr *et al.*, 2005), while the folding-based morphological indices represent the complexity of the cerebral surface (Luders *et al.*, 2006; Van Essen *et al.*, 2006; Yotter *et al.*, 2011). Interestingly, our previous study found that age-related changes in the topological organization of single-subject morphological brain networks were also mainly embodied in the CTNs (Ruan *et al.*, 2023). As MDD is associated with neurodevelopmental abnormalities in large-scale brain networks (Charlton *et al.*, 2015; Li *et al.*, 2022), it is important to explore how the CTNs deviate from normal developmental and aging trajectories in patients with MDD. In addition, we noted that the topological alterations in the CTNs were observed only nodal but not global network measures. This might be because the adolescents with MDD recruited in this study were at the early stage of the disease (median course of illness 6 months), which is not enough to disrupt the topological organization of single-subject morphological brain networks at a global level. Finally, our analysis of local cortical morphology revealed no significant alterations in any regions. This finding lends support to the popular view of MDD as a network dysfunctional syndrome (Gong & He, 2015), and highlights the important roles of network analysis in studies of adolescent MDD.

There were several limitations in this study. First, the sample size was small because it was difficult to recruit first-episode, treatment-naive adolescents with MDD in China. In addition, our correlation results were not corrected for multiple comparisons. Thus, the findings observed in this study should be considered as exploratory, and need to be validated by independent, large-sample studies in the future. Second, this study concerned exclusively the topological alterations of morphological brain networks in adolescent MDD. To what extent the alterations are similar to those derived from functional and structural brain networks should be illustrated by future multimodal studies. In particular, it is interesting to examine whether combining different types of brain networks can improve the discriminant accuracy of adolescent MDD. Finally, there are several different methods for constructing single-subject morphological brain networks (Seidlitz *et al.*, 2018; Tijms *et al.*, 2012; Wang *et al.*, 2016; Yu *et al.*, 2018). A natural topic is to test which method is the most sensitive in detecting adolescent MDD-related alterations to help individualized diagnosis of the disease.

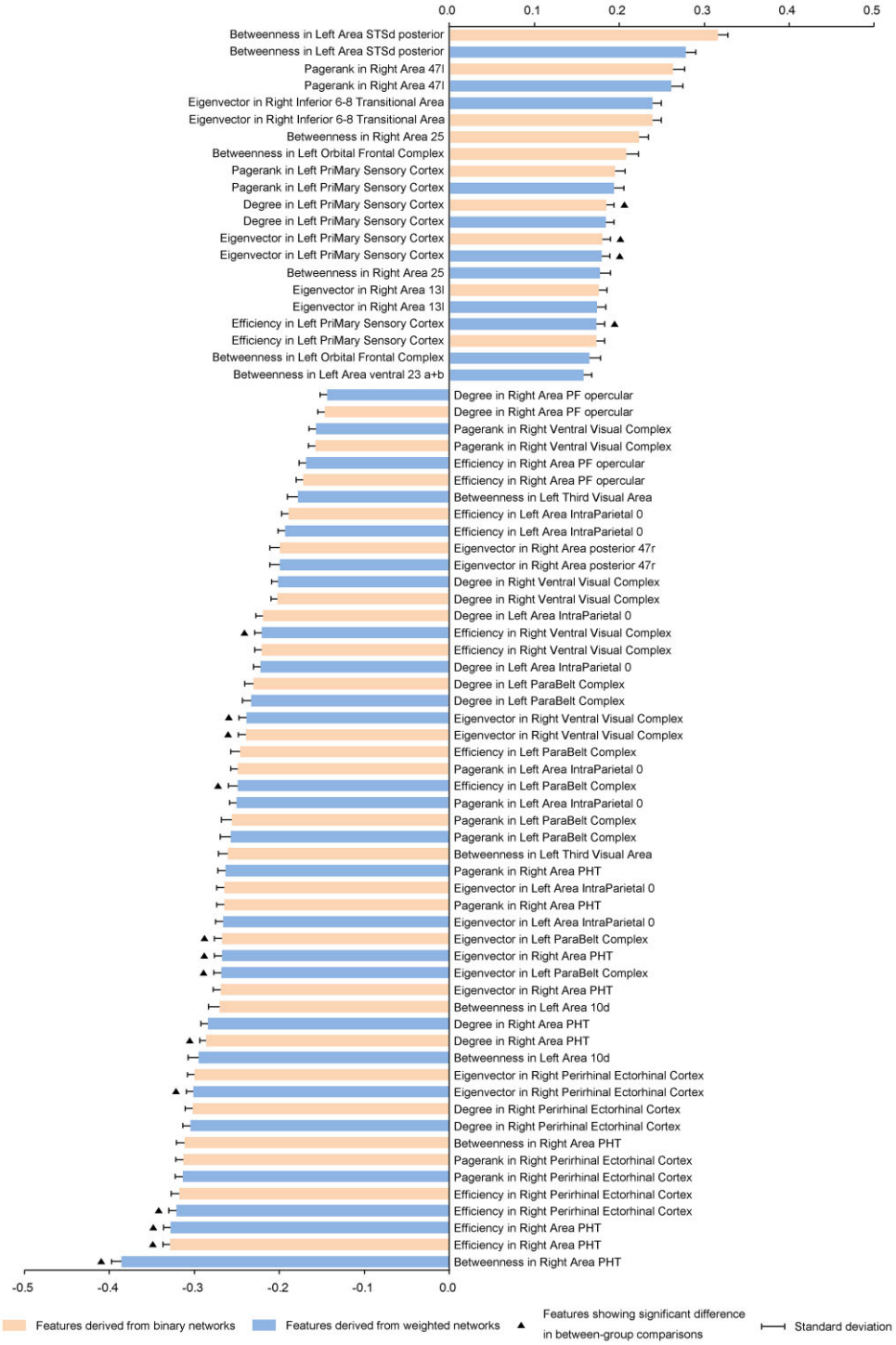

Figure 4: Consistent network properties derived from the CTNs that were selected to train the SVM classifiers. Seventy-three properties were consistently selected to train the SVM classifiers across all folds and repeats. The properties were mainly involved in frontal and parietal regions in addition to those showing significant between-group differences.

Conclusion

In this study, we explored the topological alterations of morphological brain networks in adolescents with MDD. Compared with the HCs, the adolescents with MDD showed increased nodal centralities in parietal but decreased nodal centralities in temporal regions in the CTNs. The alterations were related to cognitive deficits and clinical characteristics of the patients and could distinguish the patients from HCs. These findings may help understand the neuropathology of adolescent MDD and the observed alterations may serve as potential biomarkers to help diagnose and monitor the disease.

Author contributions

Xiaofan Qiu (Formal analysis, Visualization, Writing – original draft), Junle Li (Formal analysis), Fen Pan (Data curation), Yuping Yang (Formal analysis), Weihua Zhou (Data curation), Jinkai Chen (Data curation), Ning Wei (Data curation), Shaojia Lu (Data curation), Xuchu Weng (Writing – review & editing), Manli Huang (Conceptualization), and Jinhui Wang (Conceptualization, Formal analysis, Funding acquisition, Methodology, Writing – review & editing)

Conflict of Interests

The authors declare that they have no known competing financial interests or personal relationships that could have appeared to influence the work reported in this paper.

Acknowledgements

This work was supported by the Key-Area Research and Development Program of Guangdong Province (No. 2019B030335001), National Natural Science Foundation of China (Nos. 81922036), Key Realm R&D Program of Guangzhou (No. 202007030005), and Natural Science Foundation of Guangdong Province (2021A1515010746).

Data Availability

The data that support the findings of this study are available from the corresponding author upon reasonable request.

Reference

Achard S (2006) A resilient, low-frequency, small-world Human brain functional network with highly connected association cortical hubs. *J Neurosci* **26**:63–72.

Ahern E, Semkovska M (2017) Cognitive functioning in the first-episode of major depressive disorder: a systematic review and meta-analysis. *Neuropsychology* **31**:52–72.

Arnett JA, Labovitz SS (1995) Effect of physical layout in performance of the trail making test. *Psychol Assess* **7**:220–1.

Ashburner J, Friston KJ (2011) Diffeomorphic registration using geodesic shooting and Gauss–Newton optimisation. *Neuroimage* **55**:954–67.

Baddeley A (1992) Working memory. *Science* **255**:556–9.

Baggio HC, Abos A, Segura B, *et al.* (2018) Statistical inference in brain graphs using threshold-free network-based statistics. *Hum Brain Mapp* **39**:2289–302.

Balvin N, Banati P (2017) *The Adolescent Brain: a Second Window to Opportunity—A Compendium*. Florence: UNICEF. Retrieved August 28, 2021, from https://www.unicef-irc.org/publications/933-the-adolescent-brain-a-second-window-of-opportunity-a-compendium.html

Belcher BR, Zink J, Azad A, *et al.* (2021) The roles of physical activity, exercise, and fitness in promoting resilience during adolescence: effects on mental well-being and brain development. *Biol Psychiatry Cogn Neurosci Neuroimaging* **6**:225–37.

Blumenfeld H. (2016) Neuroanatomical Basis of Consciousness. *The Neurology of Conciousness*(pp.3–29). Elsevier Academic Press. Retrieved November 4, 2021, from https://linkinghub.elsevier.com/retrieve/pii/B9780128009482000017

Bromet E, Andrade LH, Hwang I, *et al.* (2011) Cross-national epidemiology of DSM-IV major depressive episode. *BMC Medicine* **9**:90.

Bubl E, Kern E, Ebert D, *et al.* (2010) Seeing gray when feeling blue? Depression can be measured in the eye of the diseased. *Biol Psychiatry* **68**:205–8.

Cai M, Ma J, Wang Z, *et al.* (2023) Individual-level brain morphological similarity networks: current methodologies and applications. *CNS Neurosci Ther* 1–12.

Casas-Roma J, Martinez-Heras E, Solé-Ribalta A, *et al.* (2022) Applying multilayer analysis to morphological, structural, and functional brain networks to identify relevant dysfunction patterns. *Network Neurosci* **6**:916–33.

Charlton RA, Leow A, GadElkarim J, *et al.* (2015) Brain connectivity in late-life depression and aging revealed by network analysis. *Am J Geriatr Psychiatry* **23**:642–50.

Chen T, Kendrick KM, Wang J, *et al.* (2017) Anomalous single-subject based morphological cortical networks in drug-naive, first-episode major depressive disorder: individual brain morphological networks in MDD. *Hum Brain Mapp* **38**:2482–94.

Chu S-H, Lenglet C, Schreiner MW, *et al.* (2018) Biomarkers for adolescent MDD from anatomical connectivity and network topology using diffusion MRI. *2018 40th Annual International Conference of the IEEE Engineering in Medicine and Biology Society (EMBC)*(pp. 1152–5). Presented at the 2018 40th Annual International Conference of the IEEE Engineering in Medicine and Biology Society (EMBC), Honolulu, HI: IEEE. Retrieved March 6, 2022, from https://ieeexplore.ieee.org/document/8512505/

Collorone S, Prados F, Hagens MH, *et al.* (2020) Single-subject structural cortical networks in clinically isolated syndrome. *Multiple Sclerosis J* **26**:1392–401.

Dahnke R, Yotter RA, Gaser C (2013) Cortical thickness and central surface estimation. *Neuroimage* **65**:336–48.

Doom JR, Gahagan S, Caballero G, *et al.* (2021) Infant iron deficiency, iron supplementation, and psychosocial stress as predictors of neurocognitive development in Chilean adolescents. *Nutr Neurosci* **24**:520–9.

Fallucca E, MacMaster FP, Haddad J, *et al.* (2011) Distinguishing between major depressive disorder and obsessive-compulsive disorder in children by measuring regional cortical thickness. *Arch Gen Psychiatry* **68**:527.

Ferrari AJ, Somerville AJ, Baxter AJ, *et al.* (2013) Global variation in the prevalence and incidence of major depressive disorder: a systematic review of the epidemiological literature. *Psychol Med* **43**:471–81.

Gao J, Chen M, Xiao D, *et al.* (2023) Classification of major depressive disorder using an attention-guided unified deep convolutional neural network and individual structural covariance network. *Cereb Cortex* **33**:2415–25.

Glasser MF, Coalson TS, Robinson EC, *et al.* (2016) A multi-modal parcellation of human cerebral cortex. *Nature* **536**:171–8.

Gong Q, He Y (2015) Depression, neuroimaging and connectomics: a selective overview. *Biol Psychiatry* **77**:223–35.

Gotlib IH, Joormann J (2010) Cognition and depression: current status and future directions. *Ann Rev Clin Psych* **6**:285–312.

Greenberg PE, Fournier A-A, Sisitsky T, *et al.* (2015) The economic burden of adults with major depressive disorder in the United States (2005 and 2010). *J Clin Psychiatry* **76**:155–62.

Hamilton M (1967) Development of a rating scale for primary depressive illness. *Br J Soc Clin Psychol* **6**:278–96.

He Y, Chen ZJ, Evans AC (2007) Small-world anatomical networks in the human brain revealed by cortical thickness from MRI. *Cereb Cortex* **17**:2407–19.

Ho TC, Sacchet MD, Connolly CG, *et al.* (2017) Inflexible functional connectivity of the dorsal anterior cingulate cortex in adolescent major depressive disorder. *Neuropsychopharmacology* **42**:2434–45.

Ho TC, Zhang S, Sacchet MD, *et al.* (2016) Fusiform gyrus dysfunction is associated with perceptual processing efficiency to emotional faces in adolescent depression: a model-based approach. *Front Psych* **7**:40.

Huang M, Luo B, Hu J, *et al.* (2012) Repetitive transcranial magnetic stimulation in combination with citalopram in young patients with first-episode major depressive disorder: a double-blind, randomized, sham-controlled trial. *Aus NZ J Psychiatry* **46**:257–64.

Jiang J, Zhou H, Duan H, *et al.* (2017) A novel individual-level morphological brain networks constructing method and its evaluation in PET and MR images. *Heliyon* **3**:e00475.

Jiang X, Shen Y, Yao J, *et al.* (2019) Connectome analysis of functional and structural hemispheric brain networks in major depressive disorder. *Transl Psychiatry* **9**:136.

Johnson D, Dupuis G, Piche J, *et al.* (2018) Adult mental health outcomes of adolescent depression: a systematic review. *Depress Anxiety* **35**:700–16.

Kaas JH, Hackett TA (2000) Subdivisions of auditory cortex and processing streams in primates. *Proc Natl Acad Sci USA* **97**:11793–9.

Kong X, Liu Z, Huang L, *et al.* (2015) Mapping individual brain networks using statistical similarity in regional morphology from MRI. *PLoS ONE* **10**:e0141840.

Korgaonkar MS, Goldstein-Piekarski AN, Fornito A, Williams LM (2020) Intrinsic connectomes are a predictive biomarker of remission in major depressive disorder. *Mol Psychiatry* **25**:1537–49.

Lenroot RK, Giedd JN (2006) Brain development in children and adolescents: insights from anatomical magnetic resonance imaging. *Neurosci Biobehav Rev* **30**:718–29.

Leppänen JM (2006) Emotional information processing in mood disorders: a review of behavioral and neuroimaging findings. *Curr Opin Psychiatry* **19**:34–9.

Li J, Huang M, Pan F, *et al.* (2022) Aberrant development of cross-frequency multiplex functional connectome in first-episode, drug-naive major depressive disorder and schizophrenia. *Brain Connect* **12**:538–48.

Li J, Seidlitz J, Suckling J, *et al.* (2021) Cortical structural differences in major depressive disorder correlate with cell type-specific transcriptional signatures. *Nat Commun* **12**:1647.

Li W, Yang C, Shi F, *et al.* (2017) Construction of individual morphological brain networks with multiple morphometric features. *Front Neuroanatomy* **11**:34.

Li X, Wang J (2021) Abnormal neural activities in adults and youths with major depressive disorder during emotional processing: a meta-analysis. *Brain Imag Behav* **15**:1134–54.

Li Y, Chu T, Liu Y, *et al.* (2023) Classification of major depression disorder via using minimum spanning tree of individual high-order morphological brain network. *J Affect Disord* **323**:10–20.

Li Y, Wang N, Wang H, *et al.* (2021c) Surface-based single-subject morphological brain networks: effects of morphological index, brain parcellation and similarity measure, sample size-varying stability and test-retest reliability. *Neuroimage* **235**:118018.

Li Z, Li J, Wang N, *et al.* (2022) Cortical morphological Brain networks: phenotypic associations and microbiological substrates. *SSRN Electronic J* Retrieved August 13, 2023, from http://dx.doi.org/10.2139/ssrn.4094329

Luders E, Thompson PM, Narr KL, *et al.* (2006) A curvature-based approach to estimate local gyrification on the cortical surface. *Neuroimage* **29**:1224–30.

Lv Y, Wei W, Han X, *et al.* (2021) Multiparametric and multilevel characterization of morphological alterations in patients with transient ischemic attack. *Hum Brain Mapp* **42**:2045–60.

Maletic V, Robinson M, Oakes T, *et al.* (2007) Neurobiology of depression: an integrated view of key findings: neurobiology of depression. *Int J Clin Pract* **61**:2030–40.

Mao N, Che K, Chu T, *et al.* (2020) Aberrant resting-State brain function in adolescent depression. *Front Psychol* **11**:1784.

Meruelo AD, Brumback T, Nagel BJ, *et al.* (2021) Neuroimaging markers of adolescent depression in the National Consortium on Alcohol and Neurodevelopment in Adolescence (NCANDA) study. *J Affect Disord* **287**:380–6.

Monchi O, Petrides M, Petre V, *et al.* (2001) Wisconsin card sorting revisited: distinct neural circuits participating in different stages of the task identified by event-related functional magnetic resonance imaging. *J Neurosci* **21**:7733–41.

Nardi B, Francesconi G, Catena-Dell'Osso M, Bellantuono C (2013) Adolescent depression: clinical features and therapeutic strategies. *Eur Rev Med Pharmacol Sci* **17**:1546–51.

Narr KL, Bilder RM, Toga AW, *et al.* (2005) Mapping cortical thickness and gray matter concentration in first episode schizophrenia. *Cereb Cortex* **15**:708–19.

Otte C, Gold SM, Penninx BW, *et al.* (2016) Major depressive disorder. *Nat Rev Dis Primers* **2**:16065.

Pan F, Xu Y, Zhou W, *et al.* (2020) Disrupted intrinsic functional connectivity of the cognitive control network underlies disease severity and executive dysfunction in first-episode, treatment-naive adolescent depression. *J Affect Disord* **264**:455–63.

Pollatos O, Traut-Mattausch E, Schandry R (2009) Differential effects of anxiety and depression on interoceptive accuracy. *Depress Anxiety* **26**:167–73.

Poznanski EO, Grossman JA, Buchsbaum Y, *et al.* (1984) Preliminary studies of the reliability and validity of the children's depression rating scale. *J Am Acad Child Psychiatry* **23**:191–7.

Ray D, Bezmaternykh D, Mel'nikov M, *et al.* (2021) Altered effective connectivity in sensorimotor cortices is a signature of severity and clinical course in depression. *Proc Natl Acad Sci USA* **118**:e2105730118.

Rosvold HE, Mirsky AF, Sarason I, *et al.* (1956) A continuous performance test of brain damage. *J Consult Psychol* **20**:343–50.

Ruan J, Wang N, Li J, *et al.* (2023) Single-subject cortical morphological brain networks across the adult lifespan. *Hum Brain Mapp* **44**:5429–49.

Rubinov M, Sporns O (2010) Complex network measures of brain connectivity: uses and interpretations. *Neuroimage* **52**:1059–69.

Sacchet MD, Ho TC, Connolly CG, *et al.* (2016) Large-scale hypoconnectivity between resting-State functional networks in unmedicated adolescent major depressive disorder. *Neuropsychopharmacology* **41**:2951–60.

Saenz M, Langers DRM (2014) Tonotopic mapping of human auditory cortex. *Hear Res* **307**:42–52.

Sebenius I, Seidlitz J, Warrier V, *et al.* (2023) Robust estimation of cortical similarity networks from brain MRI. *Nat Neurosci* **26**:1461–71.

Seidlitz J, Váša F, Shinn M, *et al.* (2018) Morphometric similarity networks detect microscale cortical organization and predict inter-individual cognitive variation. *Neuron* **97**:231–47. e7.

Shin J-H, Um YH, Lee CU, *et al.* (2018) Multiple cortical thickness subnetworks and cognitive impairments in first episode, drug naïve patients with late life depression: a graph theory analysis. *J Affect Disord* **229**:538–45.

Singh MK, Kesler SR, Hadi Hosseini SM, *et al.* (2013) Anomalous gray matter structural networks in major depressive disorder. *Biol Psychiatry* **74**:777–85.

Stroop JR (1935) Studies of interference in serial verbal reactions. *J Exp Psychol* **18**:643–62.

Thapar A, Collishaw S, Pine DS, Thapar AK (2012) Depression in adolescence. *Lancet North Am Ed* **379**:1056–67.

Thompson T, Correll CU, Gallop K, *et al.* (2016) Is pain perception altered in people with depression? A systematic review and meta-analysis of experimental pain research. *J Pain* **17**:1257–72.

Tijms BM, Series P, Willshaw DJ, Lawrie SM (2012) Similarity-based extraction of individual networks from gray matter MRI scans. *Cereb Cortex* **22**:1530–41.

Tymofiyeva O, Yuan JP, Huang C-Y, *et al.* (2019) Application of machine learning to structural connectome to predict symptom reduction in depressed adolescents with cognitive behavioral therapy (CBT). *NeuroImage: Clinical* **23**:101914.

Van Essen DC, Dierker D, Snyder AZ, *et al.* (2006) Symmetry of cortical folding abnormalities in Williams syndrome revealed by surface-based analyses. *J Neurosci* **26**:5470–83.

Vos T, Allen C, Arora M, *et al.* (2016) Global, regional, and national incidence, prevalence, and years lived with disability for 310 diseases and injuries, 1990–2015: a systematic analysis for the Global Burden of Disease Study 2015. *Lancet North Am Ed* **388**:1545–602.

Wang H, Jin X, Zhang Y, Wang J (2016) Single-subject morphological brain networks: connectivity mapping, topological characterization and test–retest reliability. *Brain Behav* **6**:e00448.

Wang J, Wang L, Zang Y, *et al.* (2009) Parcellation-dependent small-world brain functional networks: a resting-state fMRI study. *Hum Brain Mapp* **30**:1511–23.

Wang J, Wang X, Xia M, *et al.* (2015) GRETNA: a graph theoretical network analysis toolbox for imaging connectomics. *Front Hum Neurosci* **9**:386.

Wang X, Cheng B, Roberts N, *et al.* (2021) Shared and distinct brain fMRI response during performance of working memory tasks in adult patients with schizophrenia and major depressive disorder. *Hum Brain Mapp* **42**:5458–76.

Wang X-H, Jiao Y, Li L (2018) Mapping individual voxel-wise morphological connectivity using wavelet transform of voxel-based morphology(N. Bergsland, ed.). *PLoS ONE* **13**:e0201243.

Watts DJ, Strogatz SH (1998) Collective dynamics of 'small-world' networks. *Nature* **393**:440–2.

Weiner KS, Golarai G, Caspers J, *et al.* (2014) The mid-fusiform sulcus: a landmark identifying both cytoarchitectonic and functional divisions of human ventral temporal cortex. *Neuroimage* **84**:453–65.

Wu B, Li X, Zhou J, *et al.* (2020) Altered whole-brain functional networks in drug-naïve, first-episode adolescents with major depression disorder. *J Magn Reson Imaging* **52**:1790–8.

Yang S, Wagstyl K, Meng Y, *et al.* (2021) Cortical patterning of morphometric similarity gradient reveals diverged hierarchical organization in sensory-motor cortices. *Cell Rep* **36**:109582.

Yang Y, Li J, Li T, *et al.* (2023) Cerebellar connectome alterations and associated genetic signatures in multiple sclerosis and neuromyelitis optica spectrum disorder. *J Transl Med* **21**:352.

Yao Z, Zou Y, Zheng W, *et al.* (2019) Structural alterations of the brain preceded functional alterations in major depressive disorder patients: evidence from multimodal connectivity. *J Affect Disord* **253**:107–17.

Yin G, Li T, Jin S, *et al.* (2023) A comprehensive evaluation of multicentric reliability of single-subject cortical morphological networks on traveling subjects. *Cereb Cortex* **33**:9003–19.

Yotter RA, Nenadic I, Ziegler G, *et al.* (2011) Local cortical surface complexity maps from spherical harmonic reconstructions. *Neuroimage* **56**:961–73.

Yu K, Wang X, Li Q, *et al.* (2018) Individual morphological brain network construction based on multivariate euclidean distances between brain regions. *Front Human Neurosci* **12**:204.

Zachlod D, Rüttgers B, Bludau S, *et al.* (2020) Four new cytoarchitectonic areas surrounding the primary and early auditory cortex in human brains. *Cortex* **128**:1–21.

Zhang Y, Liu X, Hou Z, *et al.* (2021) Global topology alteration of the brain functional network affects the 8-week antidepressant response in major depressive disorder. *J Affect Disord* **294**:491–6.

Zhao K, Zheng Q, Che T, *et al.* (2021) Regional radiomics similarity networks (R2SNs) in the human brain: reproducibility, small-world properties and a biological basis. *Network Neuroscience* **5**:783–97.

Received: 5 June 2023; **Revised:** 13 September 2023; **Accepted:** 20 September 2023